DOI 10.5162/sensoren2019/P2.18

Characterization of the single point precision of steel gear wheel measurements using tactile coordinate measurement machines in scanning mode

Andreas Michael Müller[1], Sebastian Metzner[1], Tino Hausotte[1]
[1]Institute of Manufacturing Metrology (FMT), Naegelsbachstrasse 25, 91052 Erlangen, Germany

Summary

The framework of the single point uncertainty developed at the Institute of Manufacturing Metrology (FMT) presents a methodology to determine and evaluate the local measurement uncertainty for a measurement setup by local comparison of a measurement series with an associated reference geometry. This approach, which was originally developed and optimized for the processing of complete areal measurements of work pieces, was now also extended to line scans found in dimensional testing using tactile coordinate measurement machines (CMM). Target of the investigation are straight-toothed steel gear wheels, which can be dimensionally characterized by both helix and profile scans using a CMM in scanning mode in combination with a rotatory stage. The modification of the single point uncertainty framework in order to determine the single point precision of repeated gear wheel measurements was implemented successfully but the test setup also yielded abnormally high random measurement errors, which could not fully be explained within our examinations.

Keywords: gear wheel, tactile coordinate measurement, single point precision, scanning mode

Introduction

The framework of the single point uncertainty describes a methodology to statistically evaluate the local measurement uncertainty of a measurement series consisting of *n* repeated single measurements with respect to the associated reference geometry in the sense of International Vocabulary of Metrology (VIM) [1]. Usually, a geometric registration routine is required to geometrically align each of the single measurements with the reference geometry. The surface data is represented by triangle meshes using the STL file format. Originating from homogeneously distributed surface points on the reference surface (also called sampling points), the distances to each single measured surface are calculated. Depending on the sampling strategy applied, slightly different distances are computed [2]. Finally, each sampling point is associated with *n* calculated distances (one for each measurement repetition). For each set of distances, the mean value as well as the standard deviation can be computed. In case the reference geometry is known, the local systematic deviations combined with the local random deviations represent the single point (measurement) uncertainty. In case no reference measurement exists, the nominal geometry of the work piece can be used. In that case, the mean distance value represents the combination of the systematic error and the work piece deviations and both effects cannot be separated. Nonetheless, the distribution of random measurement errors (precision) of the measurement setup can be determined.

The exact knowledge of the single point uncertainty of a measurement setup result can greatly influence the quality of the subsequent measurement data evaluations. The processing of single point precision data as weighting factors in geometry element fitting routines can lead to a more accurate determination of geometry element properties [3]. For industrial computed tomography (CT), the visual evaluation of the locally varying uncertainties gives direct insight into the underlying X-ray penetration lengths. This is because they directly affect the single point noise due to the impaired signal to noise properties of the recorded projections. The method was successfully used to correct systematic measurement errors in CT measurements by determining the systematic single point errors of a simulated measurement series and subsequently correcting these systematic measurement deviations [4]. The core routine used in this former work at the Institute of Manufacturing Metrology, which is based on ray-triangle intersection tests, provided accurate results under most conditions [5]. This algorithm computes the distance from each sampling

point of the reference / nominal geometry in the direction of the vertex normal vectors of these sampling points to the triangulated measurement geometry. This sampling strategy is called “normal vector” (Fig. 1). If a measured coordinate is trustworthy, the same applies for the normal vector of the nominal geometry and thus defines the direction in which the corresponding point on a measurement surface is most likely expected. Mathematically, this problem is described by a ray-triangle intersection test, which is a well-known problem in the field of computer graphics [6–10]. Subsequent development efforts resulted in the introduction of an alternative sampling strategy, which solves the problematic sampling of edge regions associated with the sampling in the direction of the surface normal vector [2]. This sampling strategy calculates the shortest distance from a sampling point to the target surface and is therefore called “shortest distance” (Fig. 1). Additionally, this sampling exhibits superior run time properties compared to the existing ray-tracing solution. The determination of the single point uncertainty makes it then possible to pass information about the measurement uncertainty to complex extended tolerance analysis methods and therefore consider the uncertainty inherently associated with any measurement [11].

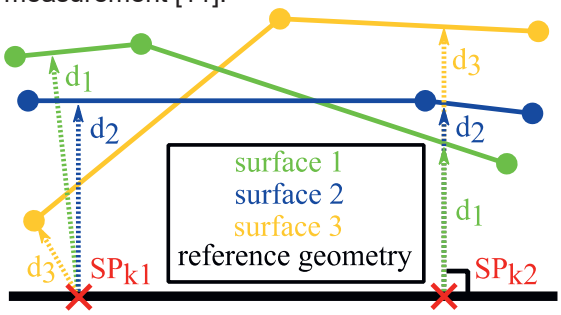

Fig. 1: Visualization of the sampling strategies “shortest distance” (left) and “normal vector” (right).

So far, we only determined and evaluated the single point uncertainties for measurement systems producing an areal measurement result represented as triangle meshes. These are mainly CT and structured-light scanning [12]. This contribution presents various suitable adjustments to the single point uncertainty framework in order to also be able to process line scans from coordinate measurement machines (CMM) using the example of gear wheel measurements.

Measurement data

For the following demonstration purposes, a wire eroded, straight-toothed steel gear wheel characterized by 17 teeth, a width of 8 mm and tip circle diameter of 19.4 mm is used. The measurement setup consists of the tactile CMM UPMC 1200 CARAT S-ACC with an included rotatory stage. The measurement data evaluation was done using the software tools Zeiss Calypso 5.6 and Zeiss Gear Pro 5.9.0.2. Contrary to areal measurements, which are typically represented by or easily converted into a triangle mesh representation, CMM line scans consist of point clouds with additional meta-information (e.g. probing vectors). With respect to gear wheel inspection, the guideline VDI/VDE 2612 states, *“Unless agreed otherwise, the profile is measured in a transverse plane approximately in the middle of the face width.”* [13]. The profile measurement is complemented by the helix measurement: *“The helix preferably is measured on the diameter of the V-cylinder.”* [13]. Summarizing, each gear flank is described by one profile scan and one helix scan. The exact scan trajectory in interaction with the rotatory stage within the presented examinations were determined by the software Zeiss Gear Pro. All controllable filter operations on the measurement data were switched off, the ball tip diameter was 0.8 mm.

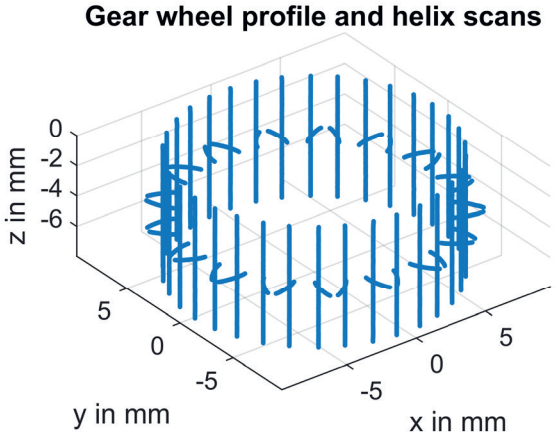

Fig. 2: Visualization of a complete tactile gear wheel measurement consisting of profile and helix scans.

Figure 2 shows the results of a complete gear wheel measurement using the described tactile measurement setup. In order to apply the single point uncertainty framework, the complete gear wheel measurement was repeated 20 times (n = 20), following the recommendation in the norm ISO 15530-3:2011 [14]. Thus, this setting theoretically results in a relative uncertainty of the investigations, caused by the limited sampling, of 16 %, assuming normally distributed uncertainties [15].
At the beginning of the measurement, the coordinate system of the gear wheel with respect to the coordinate system of the CMM was defined. First, the rotation axis of the gear wheel was de-

termined by two circle scans. The remaining rotatory symmetry was dissolved by centering of the probe stylus between two gear teeth. The measurements were performed in a temperature-controlled environment with temperatures set to 20 °C ±0.2 K (temperature classification A according to VDI/VDE 2627-1 [16]) with a relative humidity of 45 % ±10 % (humidity classification A according to VDI/VDE 2627-1 [16]).

Calculating the single point precision

As mentioned above, the single point uncertainty framework was developed to evaluate the uncertainty parameters from repeated areal measurements of measurement objects. Contrary to that, the tactile gear evaluation is characterized by line scans, thus the sampling strategy using the normal vector of the sampling start surface was not feasible. The reason for that is that in general a ray-tracing algorithm can only test the intersections of a ray with areal targets which is not the case for line scans. Consequently, the sampling strategy “shortest distance” had to be used. The measurement results of a tactile line scan are represented by the recording of m measurement points $\{X_i\}_{i=1}^{m} \subseteq \mathbb{R}^3$ as well as the associated probing vectors $\{V_i\}_{i=1}^{m} \subseteq \mathbb{R}^3$ and the distances $\{d_i\}_{i=1}^{m} \subseteq \mathbb{R}^1$ from the nominal geometry to $\{X_i\}_{i=1}^{m}$ in the direction of the probing vectors $\{V_i\}_{i=1}^{m}$. Although the nominal geometry is not given explicitly in the coordinate system of the measurement system, the nominal geometry coordinates $\{N_i\}_{i=1}^{m} \subseteq \mathbb{R}^3$ belonging to each measurement coordinate $\{X_i\}_{i=1}^{m}$ can be reconstructed as follows (1):

$$N_i = X_i - V_i \cdot d_i \tag{1}$$

In the following, $\left\{\{N_i^k\}_{i=1}^{m}\right\}_{k=1}^{n} \subseteq \mathbb{R}^3$ denotes the nominal geometry of the same line scan of all n measurements of the measurement series. Assuming a perfect measurement, the superposition of all calculated sets of nominal geometry coordinates $\left\{\{N_i^k\}_{i=1}^{m}\right\}_{k=1}^{n}$ should result in the same nominal geometry by definition. However, Fig. 3 shows that this is not the case for real measurements due to various kinds of error sources influencing the measurements. To determine the single point uncertainties, the common nominal geometry must be known, because it represents the definition of the sampling points. As a result of the pre-knowledge, that the gear wheel is straight-toothed, we know that each nominal helix geometry must be a straight line. Consequently, one possibility to reconstruct the nominal helix scan line from the repeatedly measured scans is to calculate the solution for a line regression model (Fig. 3, green line). This was done based on the singular value decomposition (SVD) of all coordinates $\left\{\{N_i^k\}_{i=1}^{m}\right\}_{k=1}^{n}$ [17], which results in a least squares solution for the scan direction vector. The position of that scan line is determined by the mean value of $\left\{\{N_i^k\}_{i=1}^{m}\right\}_{k=1}^{n}$.

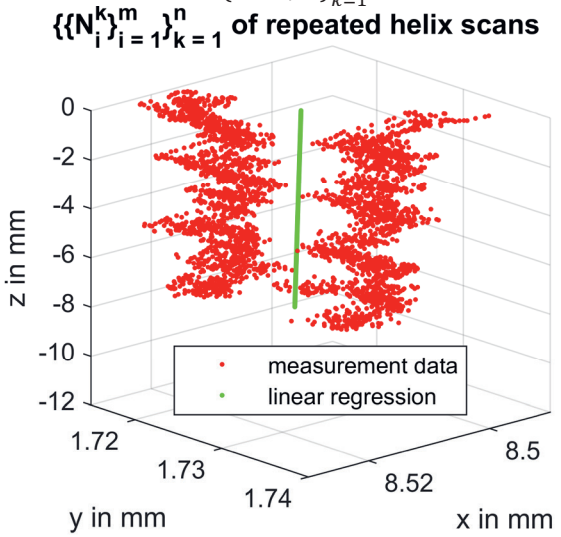

Fig. 3: Visualization of the calculated nominal geometry from repeated helix scans and the result of the linear regression. Caution: Axes are not equally scaled!

The z-components e_z of all probing vectors $\{V_i\}_{i=1}^{m}$ recorded during the measurements were always zero, thus all probing vectors are perpendicular to the scan direction e_z.

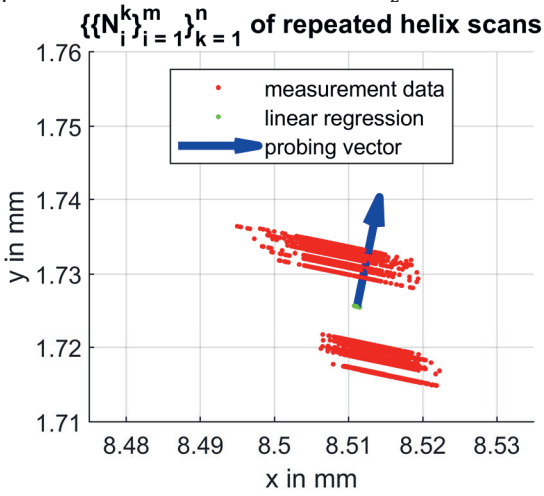

Fig. 4: Projection of the calculated nominal geometry into the xy-plane. Measurement deviations perpendicular to the probing vector (z component is zero) are not recorded.

That means that deviations from the nominal geometry perpendicular to both the probing vector and the scan direction can in principle not be

recorded for straight-line scans using only one vector $\{V_i\}_{i=1}^m$, which is also observable in Fig. 4. Consequently, the regression analysis was necessary here to reconstruct the nominal helix, which is required to sample the single point scatter. Figure 4, which contains the same measurement data as Fig. 3, also shows that the repeated scans are affected by some kind of offset relative to each other, which indicates the influence of a dominant error source within the measurement chain. After determining the nominal helix scan, sampling points were spaced out equally on that line. After that, the shortest (signed) Euclidean distances from each sampling point to each repeatedly measured helix scan defined by $\{X_i^k\}_{i=1}^m$ were calculated, resulting in the distance sets $\{t_k\}_{k=1}^n \subseteq \mathbb{R}^1$ now associated with each sampling point. The calculation also allowed for intersections between sampling points using linear interpolation and is therefore not equal to a simple nearest neighbor search. The "shortest distance" sampling also additionally requires the vertex normal vectors for each sampling point in order to decide if deviations are counted as positive or negative values. These vertex normal vectors for each sampling point, are defined by the mean vector of $\{V_i\}_{i=1}^m$. Next, the single point scatter for each sampling point was defined by the standard deviation of $\{t_k\}_{k=1}^n$. The described approach was then repeated for all helix scans. A very similar data processing pipeline was implemented to determine the nominal profile scan geometry. Here, the SVD was used to identify the two main axes of the point cloud $\left\{\{N_i^k\}_{i=1}^m\right\}_{k=1}^n$, which was then followed by a regression analysis using a high degree polynomial ($\mathbb{R}^2$) model.

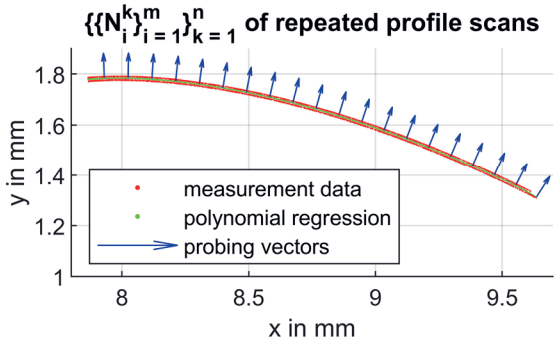

Fig. 5: Visualization of the calculated nominal geometry from repeated profile scans and the result of the high order polynomial regression (between the red lines).

Figure 5 shows the determination of the nominal profile scan line (embedded between the red lines). Note that the recorded z-components e_z of the probing vectors $\{V_i\}_{i=1}^m$ during the measurements are again always zero. After that, equally spaced sampling points are defined on that nominal geometry and the associated vertex normal vectors are calculated by derivation of the fitted function (z-components e_z set to zero). Finally, the single point scatter could then be calculated the same way as described above, which was also repeated for each of the profile scans afterwards.

Results

Figure 6 shows the calculated single point precision for all gear wheel profile and helix scans. The observed precision values represent the superimposition of all uncorrected measurement error contributions along the complete measurement chain. This includes the definition of the coordinate systems and additional components like to rotatory stage. The profile scans exhibit systematically lower precision values in the range between 2 µm and 10 µm compared to the helix scans (between 10 µm and 25 µm). Additionally, the precision noticeably fluctuates along the helix scans. For the examined measurement setup, the precision of the rotatory stage can be regarded as especially important Because of that, the rotatory stage was undertaken additional examinations, which are described in the subsequent section. Finally, the findings are discussed in the section after that.

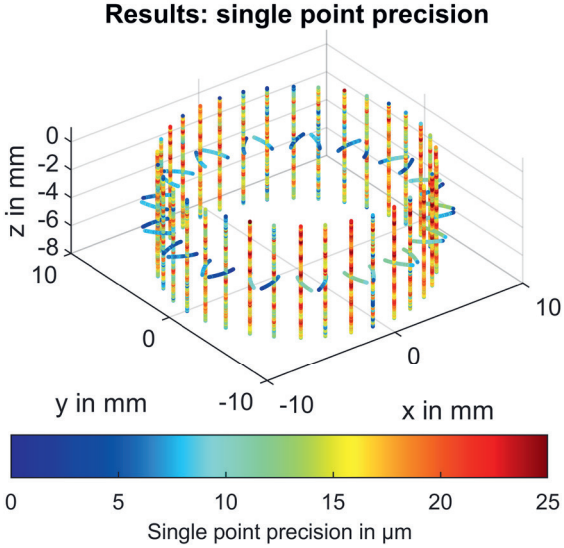

Fig. 6: Single point precision for helix and profile scans of repeated gear wheel measurements.

Testing the precision of the rotatory stage

The target of the following examination was to determine, if the error characteristics of the rotatory stage could account for the observed single point precision values. For that purpose, a

flick normal (precision cylinder with a flattening of 15 µm) was repeatedly measured 20 times. A single measurement consisted of two circle scans of the cylinder shell surface, which were used to determine the cylinder axis. Another circle scan characterizes the front surface of the cylinder and the fourth circle scan, measures the flick (flattened area). Figure 7 shows the distance of the measurement coordinates from the common Gaussian circle in Polar coordinates. The location of the flick is clearly visible at around 10° (see also Fig. 8). The flick normal was rotated by the rotatory stage during the measurement with a fixed position of the probe stylus. This approach makes the verification of the precision of the rotatory stage possible, because the measured coordinates were then effectively represented by polar coordinates (angle in xy-plane recorded by the rotatory stage and radius by the CMM). The coordinate system was arranged such that the z-axis was represented by the determined flick normal cylinder axis. Then, the measured coordinates, which are part of the flick, were extracted by an iterative distance and angle based search algorithm.

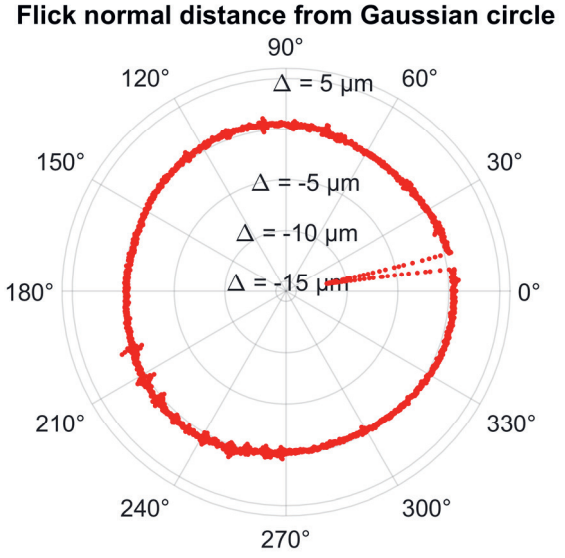

Fig. 7: Circle scan containing the flick (height 15 µm): Distances from Gaussian circle. See also coordinates in Fig. 8

Afterwards, the position of the flick was determined by robustly fitting a polynomial function (degree 1), which can be written as (2), into the selected part of the circle scan (Fig. 8).

$$f(x) = ax + b \tag{2}$$

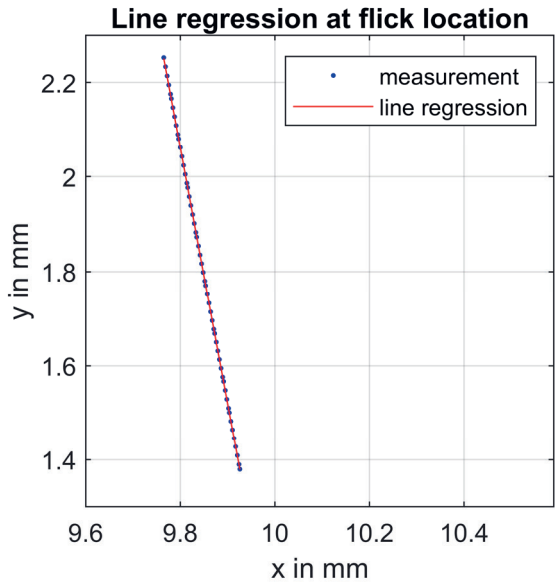

Fig. 8: Robust line regression at the flick location, same coordinate system as Fig. 7.

The angular representation of the slope (3) of that line then represents the angular position of the flick.

$$\theta = \arctan(a) \tag{3}$$

Consequently, the scatter of that angle observed over multiple repeated measurements describes the angular positioning precision of the rotatory stage.
Assuming an underlying normal distribution and targeting a level of confidence of approx. 99 %, the value of three standard deviations [15] of the angular position was determined to be 83.7 arcsec. Additionally, the probing repeatability of the measurement chain was tested by determining the scatter of the perpendicular distance of the fitted polynomial function to the cylinder axis of the flick normal. Three standard deviations were calculated as 0.41 µm. During the calibration of the rotatory stage, a wobbling angle of 24 arcsec was determined. Additionally, the angle between the rotatory axis and the CMM coordinate system was characterized by 6 arcsec. These two error sources are of systematic nature and were therefore corrected by the measurement software.

Discussion

As already mentioned during the discussion of Fig. 4, the measurement chain was affected by various sources of uncertainty which lead to the observation of scatter values up to 20 µm – 25 µm when determining the single point scatter. This could not be explained by the probing scatter of the CMM itself, which is verified by regular calibration of the measurement device,

as well as by the observed positional repeatability (0.41 µm with 99 % confidence) of the perpendicular distance between the flick feature to the cylinder axis. A substantial part of the observed single point scatter could be explained by the lack of precision of the rotatory stage. The remaining part of the observed single point scatter is caused by various other influences. It is possible, that the centering operation during the definition of the coordinate system of the gear wheel was unstable enough to be responsible for some the observed effects. Furthermore, the surface roughness is regarded as an important influence factor on the achieved measurement uncertainties, which is reflected by the fact that the surface roughness value R_z directly contributes to the measurement uncertainty using the "Virtual CMM" used for the uncertainty calculation of the used system [18]. Additionally, dynamic effects during the scan can reduce the achieved precision, which can also be observed in Fig. 6 for the helix scans, where the precision fluctuates along the scan trajectory.

In this contribution, an adjustment of the single point uncertainty framework, which had primarily been developed to evaluated areal measurements, was presented. Now, locally resolved uncertainty values can also be calculated for CMM examinations. Repeated measurements of a steel gear wheel were used to generate the measurement data. The adjustment was characterized by the additional reconstruction of the underlying nominal geometry from the measurement data. The measurement series exhibited unexpectedly large scatter, which is in general untypical for tactile CMM measurements. A large part of the observed scatter could be assigned to the uncertainty of the used rotatory stage, although the observation could not be fully explained.

Finally, the single point uncertainty framework was successfully used to determine the scatter of the complete measurement chain of repeated CMM measurements. Future research efforts need to focus on the verification of these results by examination of different measurement objects.

Acknowledgments

The authors would like to thank the German Research Foundation (DFG) for supporting the research project "FOR 2271 process-oriented tolerance management based on virtual computer-aided engineering tools" under grant number HA 5915/9-1. The authors thank the Institute of Manufacturing Technology (LFT, FAU Erlangen-Nuremberg) for providing the steel gear wheel used for demonstration purposes in this article.

References

[1] International vocabulary of metrology: Basic and general concepts and associated terms (VIM) German-English version ISO/IEC-Guide 99:2007, Corrected version 2012, 4th ed. Berlin: Beuth, 2012.

[2] A. M. Müller and T. Hausotte, "Comparison of different measures for the single point uncertainty in industrial X-ray computed tomography," in 9th Conference on Industrial Computed Tomography, 2019.

[3] A. M. Müller and T. Hausotte, "Utilization of single point uncertainties for geometry element regression analysis in dimensional X-ray computed tomography," in 9th Conference on Industrial Computed Tomography, 2019.

[4] A. M. Müller, F. Wohlgemuth, and T. Hausotte, "Simulation-based correction of systematic errors for CT measurements," in 8th Conference on Industrial Computed Tomography, 2018.

[5] M. Fleßner, A. M. Müller, D. Götz, E. Helmecke, and T. Hausotte, "Assessment of the single point uncertainty of dimensional CT measurements," in NDT.net issue Vol.21 No.02, 2016.

[6] A. S. Glassner, An introduction to ray tracing. San Francisco, Calif.: Kaufmann, 2007.

[7] H. H. Hu, Ray tracing from the ground up: A K Peters, 2007.

[8] P. Shirley and R. K. Morley, Realistic ray tracing, 2nd ed. Natick, Mass.: AK Peters, 2003.

[9] T. Möller and B. Trumbore, "Fast, Minimum Storage Ray-Triangle Intersection," Journal of Graphics Tools, vol. 2, no. 1, pp. 21–28, 1997.

[10] C. Schlick and G. Subrenat, "Ray Intersection of Tessellated Surfaces: Quadrangles versus Triangles," in Graphics Gems 1993, pp. 232–241.

[11] A. M. Müller, T. Oberleiter, K. Willner, and T. Hausotte, "Implementation of parameterized work piece deviations and measurement uncertainties into performant meta-models for an improved tolerance specification," Proceedings of the International Conference on Engineering Design, ICED, 2019.

[12] A. M. Müller, S. Metzner, T. Hausotte, D. Schubert, and D. Drummer, "Separation of locally determined work piece deviations and measurement uncertainties for structured-light scanning of customized polymer gear wheels," in 20. GMA/ITG-Fachtagung Sensoren und Messsysteme, 2019.

[13] Measurement and testing of gears, VDI/VDE 2612 Part 1, 2018.

[14] Geometrical product specifications (GPS) -- Coordinate measuring machines (CMM): Technique for determining the uncertainty of measurement, ISO 15530-3:2011, 2018.

[15] Joint Committee for Guides in Metrology (JCGM/WG 1), Guide to the expression of uncertainty in measurement: JCGM 100:2008 - GUM 1995 with minor corrections, 2008.

[16] Measuring rooms - Classification and characteristics - Planning and execution, VDI/VDE 2627 Part 1, 2015.

[17] C. M. Shakarji and V. Srinivasan, "Theory and algorithms for weighted total least-squares fit-

ting of lines, planes, and parallel planes to support tolerancing standards," Journal of Computing and Information Science in Engineering, vol. 13, no. 3, 2013.

[18] F. Wäldele and H. Schwenke, "Automatische Bestimmung der Messunsicherheiten auf KMGs auf dem Weg in die industrielle Praxis (Automated Calculation of Measurement Uncertainties on CMMs – Towards Industrial Application)," tm - Technisches Messen Plattform für Methoden, Systeme und Anwendungen der Messtechnik, vol. 69, no. 12/2002, p. 550, http://www.degruyter.com/downloadpdf/j/teme.2002.69.issue-12_2002/teme.2002.69.12.550/teme.2002.69.12.550.xml, 2002.